REYNOLDS STRESS MODELING OF OPEN-CHANNEL FLOWS OVER BEDFORMS

Sung-Uk Choi[1] and Hyeongsik Kang[2]

[1] Associate Professor, School of Civil & Environmental Engineering, Yonsei University, Seoul 120-749, Korea

[2] Graduate Student, School of Civil & Environmental Engineering, Yonsei University, Seoul 120-749, Korea

Abstract: This paper presents a non-isotropic turbulence modeling of flows over bedforms. The Reynolds stress model is used for the turbulence closure. In the model, Launder, Reece, and Rodi's model and Hanjalic and Launder's model are employed for the pressure strain correlation term and the diffusion term, respectively. The mean flow and turbulence structures are simulated and compared with profiles measured in the experiments. The numerical solutions from two-equation turbulence models are also provided for comparisons. The Reynolds stress model yields the separation length of eddy similar to the other numerical results. Using the developed model, the resistance coefficients are also estimated for the flows at different Froude numbers. Karim's (1999) relationship is used to determine the bedform geometry. It is found that the values of the form drag and the skin friction are very similar to those obtained by the other turbulence models, meaning higher values of the form drag and lower values of the skin friction compared with the empirical formulas

Keywords: non-isotropic turbulence model, Reynolds stress model, bedforms, form drag, skin friction

1. INTRODUCTION

Most alluvial streams have bedforms on the channel bed. Hydraulically, the role of bedforms is to increase resistance to a value well above that without bedforms. Bedforms interact with the flow and determine their geometric dimensions. Ripples, dunes, plane bed, anti-dunes, and chutes and pools are different types of bedforms. Assessing resistance by bedforms is important in predicting the stage during the flood and the relevant amount of sediment transported. Recently, sediment transport by streams over bedforms emerges as a significant issue in ecohydraulics with the recognition that the transported particles can provide or destruct wildlife habitats in the stream.

Bedforms on the streambed provide resistance by means of the skin friction and form drag. The skin friction depends on the size of the bed particles, and the form drag depends on the flow structure made over bedforms. That is, the flow separation and reattachment over bedforms creates negative pressure on the bed, and determines the intensity of the form drag.

A schematic sketch of a flow over bedform is

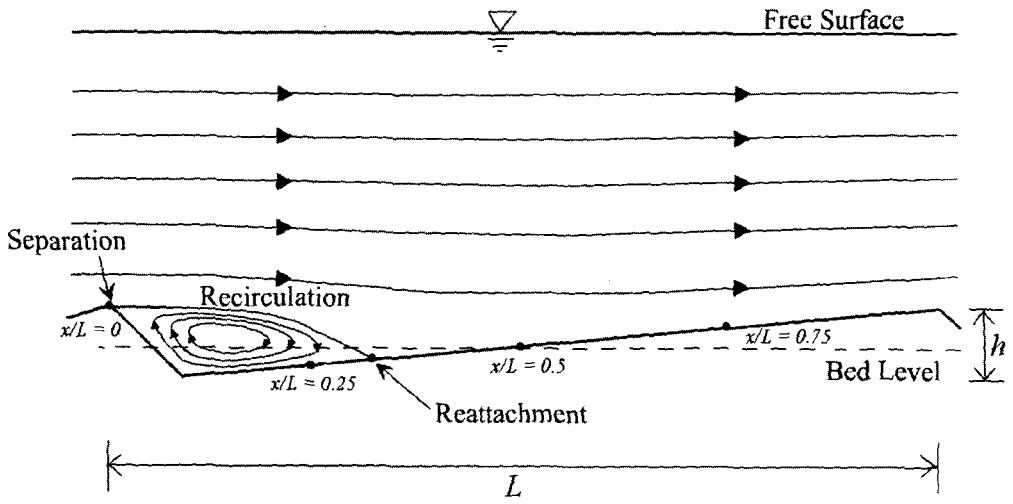

Figure 1. Flow Characteristics over Bedforms

shown in Figure 1. The flow attached to the bottom boundary tends to accelerate after leaving the trough of bedform. At the crest of bedform, the flow is separated causing the momentum loss, which is quite similar to the wake formed behind the cylinder. The flow separated at the crest shows reattachment after some distance which highly depends on the bedform height. Recirculation occurs in the separation zone, from the point of separation to the point of reattachment, and it creates the pressure difference or form drag.

Choi et al. (2002) combined the method of computational fluid dynamics with the formula for the characteristics of bedform geometry to investigate the impact of flow parameters and bottom sediment on flow resistance. They used Yoon and Patel's (1996) model for the numerical method and Karim's (1999) model for the bedform geometry. Therein, Choi et al. found that the numerical simulations result in higher values of the form drag and lower values of the skin friction compared with the empirical formulas. Possible reasons are non-isotropic effect of turbulence, ignorance of particle movement over bedform, bedform movement in the downstream direction, and 3D geometry of bedforms. In this paper, we apply a non-isotropic turbulence model to the simulation of flows over bedforms. The Reynolds stress model (RSM) is used with Launder, Reece, and Rodi's model for the pressure strain correlation term and the Hanjalic and Launder's model for the diffusion term. This model is validated by comparisons with the other turbulence models as well as with the measured profiles. The predicted flow structure over bedform, including separation and reattachment, is compared with that by the k-ω model and by the k-ε model. The impact of Froude number on flow resistance is also investigated, and comparisons are made with the empirical relationships.

2. SECOND-ORDER CLOSURE MODELS

In the present study, the Reynolds equations averaged over time are solved. The continuity

and momentum equations are respectively given by

$$\frac{\partial u_i}{\partial x_i} = 0 \tag{1}$$

$$\frac{\partial u_i}{\partial t} + u_j \frac{\partial u_i}{\partial x_j} = -\frac{1}{\rho}\frac{\partial p}{\partial x_i} + \frac{\partial}{\partial x_j}\left(\nu \frac{\partial u_i}{\partial x_j} - \overline{u_i' u_j'}\right) \tag{2}$$

where ρ is the water density, u_i is the mean velocity component in the i-direction, p is the dynamic pressure, and $-\overline{u_i' u_j'}$ is the Reynolds stress.

2.1 Two-Equation Turbulence Model

The $k-\varepsilon$ model and the $k-\omega$ model belong to the class of two-equation turbulence models, in which model transport equations are solved for two turbulence quantities, i.e., k and ε in the $k-\varepsilon$ model and k and ω in the $k-\omega$ model. In the two-equation turbulence model, the Reynolds stress is estimated by the eddy viscosity concept such as

$$-\overline{u_i' u_j'} = \nu_t\left(\frac{\partial u_i}{\partial x_j} + \frac{\partial u_j}{\partial x_i}\right) - \frac{2}{3}\delta_{ij}k \tag{3}$$

where ν_t is the eddy viscosity, δ_{ij} is the Kronecker delta, and k is the turbulent kinetic energy. The $k-\varepsilon$ model uses the following Prandtl-Kolmogorov relationship for the eddy viscosity:

$$\nu_t = C_\mu \frac{k^2}{\varepsilon} \tag{4}$$

in which C_μ is an empirical constant and ε is the turbulence kinetic energy dissipation rate. Solving the following transport equations gives the distributions of k and ε, respectively:

$$\frac{\partial k}{\partial t} + u_j \frac{\partial k}{\partial x_j} = \frac{\partial}{\partial x_j}\left(\frac{\nu_{eff}}{\sigma_k}\frac{\partial k}{\partial x_j}\right) + P - \varepsilon \tag{5}$$

$$\frac{\partial \varepsilon}{\partial t} + u_j \frac{\partial \varepsilon}{\partial x_j} = \frac{\partial}{\partial x_j}\left(\frac{\nu_{eff}}{\sigma_\varepsilon}\frac{\partial \varepsilon}{\partial x_j}\right) + C_{1\varepsilon}\frac{\varepsilon}{k}P - C_{2\varepsilon}\frac{\varepsilon^2}{k} \tag{6}$$

where ν_{eff} is the effective viscosity which is the sum of laminar viscosity (ν) and eddy viscosity (ν_t), σ_k, σ_ε, $C_{1\varepsilon}$ and $C_{2\varepsilon}$ are empirical constants, and P is the generation term given by

$$P = -\overline{u_i' u_j'}\frac{\partial u_i}{\partial x_j} \tag{7}$$

In the present computation, the following standard values by Launder and Spalding (1974) are used: $C_\mu = 0.09$, $\sigma_k = 1.0$, $\sigma_\varepsilon = 1.3$, $C_{1\varepsilon} = 1.44$, and $C_{2\varepsilon} = 1.92$.

The k-ω turbulence model is also based upon the eddy viscosity concept. Another expression of eq.(4) is given by

$$\nu_t = \gamma^* \frac{k}{\omega} \tag{8}$$

where ω denotes the specific dissipation rate ($= \varepsilon/(\beta^* k)$), which is the ratio of the turbulence dissipation rate (ε) to the turbulence kinetic energy (k). In eq.(8), such values as $\beta^* = 0.09$ and $\gamma^* = 1$ are used herein. The distributions of k and ω are obtained by solving k and ω transport equations, respectively (Wilcox, 1988).

$$\frac{\partial k}{\partial t} + u_j \frac{\partial k}{\partial x_j} = \frac{\partial}{\partial x_j}\left[(\nu + \sigma^* \nu_t)\frac{\partial k}{\partial x_j}\right] + P - \beta^* \omega k \tag{9}$$

$$\frac{\partial \omega}{\partial t} + u_j \frac{\partial \omega}{\partial x_j} = \frac{\partial}{\partial x_j}\left[(\nu + \sigma \nu_t)\frac{\partial \omega}{\partial x_j}\right] + \frac{\gamma \omega}{k} P - \beta \omega^2 \quad (10)$$

where $\sigma = \sigma^* = 0.5$, $\beta = 3/40$, and $\gamma = 5/9$.

The k-ω model is known to perform better than other two equation models especially in the inner region because of the Dirichlet type of boundary condition for the specific dissipation rate. Detailed expressions for the wall boundary are given in Wilcox (1988). In the computation, the effective roughness height is set to the median size of particles, i.e., $k_s = D_{50}$, and a symmetric condition is used for the free-surface boundary.

2.2 Reynolds Stress Model

The RSM estimates the Reynolds stress component in eq.(2) by solving their transport equations of the following form:

$$\frac{DR_{ij}}{Dt} = P_{ij} + D_{ij} - \varepsilon_{ij} + \Pi_{ij} \quad (11)$$

where R_{ij} is the Reynolds stress ($= \overline{u_i' u_j'}$), P_{ij} is the rate of production of R_{ij}, D_{ij} is the turbulent diffusion, ε_{ij} is the rate of dissipation of R_{ij}, and Π_{ij} is the pressure-strain correlation. In eq.(11), the rate of stress production of R_{ij} is given by

$$P_{ij} = -\left(R_{ik}\frac{\partial u_j}{\partial x_k} + R_{jk}\frac{\partial u_i}{\partial x_k}\right) \quad (12)$$

which does not require modeling while the remaining terms need modeling. For D_{ij}, the following model proposed by Hanjalic and Launder (1972) is used:

$$D_{ij} = C_s \frac{\partial}{\partial x_k}\left[\frac{k}{\varepsilon}\left(R_{il}\frac{\partial R_{jk}}{\partial x_l} + R_{jl}\frac{\partial R_{ik}}{\partial x_l} + R_{kl}\frac{\partial R_{ij}}{\partial x_l}\right)\right] \quad (13)$$

with $C_s = 0.11$. Most models for ε_{ij} are isotropic ones which are recognized to be incorrect near the solid boundary. Thus, herein, the following Rotta's (1951) model is used for the rate of dissipation of R_{ij}:

$$\varepsilon_{ij} = \frac{\varepsilon}{k} R_{ij} \quad (14)$$

The turbulent kinetic energy dissipation rate (ε) is obtained from its transport equation of the following form:

$$\frac{\partial \varepsilon}{\partial t} + u_i \frac{\partial \varepsilon}{\partial x_i} = \frac{\partial}{\partial x_k}\left(C_\varepsilon \frac{k}{\varepsilon}\overline{u_k' u_l'}\frac{\partial \varepsilon}{\partial x_l}\right) + C_{1\varepsilon}\frac{\varepsilon}{k}P - C_{2\varepsilon}\frac{\varepsilon^2}{k} \quad (15)$$

where C_ε is an empirical constant set equal to 0.15.

The last term in eq.(11) acts to redistribute the turbulence kinetic energy among the Reynolds normal stresses. It is customary to consider this term as being formed from three separate contributions, i.e.,

$$\Pi_{ij} = \Pi_{ij,1} + \Pi_{ij,2} + \Pi_{ij,w} \quad (16)$$

where $\Pi_{ij,1}$, $\Pi_{ij,2}$, and $\Pi_{ij,w}$ represent purely turbulent interactions, interactions between the mean strain field and fluctuating velocities, and damping effects of a solid wall, respectively. Most Reynolds stress models include the turbulent interaction term, and we use the following relationship proposed by Rotta (1951):

$$\Pi_{ij,1} = -C_1 \frac{\varepsilon}{k}\left(R_{ij} - \frac{2}{3}k\delta_{ij} \right) \tag{17}$$

with C_1 = 1.5. For $\Pi_{ij,2}$, the following model proposed by Launder et al. (1975) is used in the numerical implementation:

$$\Pi_{ij,2} = -\frac{C_2+8}{11}\left(P_{ij} - \frac{2}{3}\delta_{ij}P \right) - \frac{30C_2-2}{55}k\left(\frac{\partial u_i}{\partial x_j} + \frac{\partial u_j}{\partial x_i} \right) + \frac{8C_2-2}{11}\left(R_{ik}\frac{\partial u_k}{\partial x_j} + R_{jk}\frac{\partial u_j}{\partial x_k} + \frac{2}{3}\delta_{ij}P \right) \tag{18}$$

with $C_2 = 0.6$.

Near the bottom boundary, the fluctuating velocities normal to the bed is damped, while the fluctuating velocities parallel to the bed is enhanced. Therefore, a wall correction term needs to be added to the pressure strain model. We used the following relationship, which is a combined form of relationships by Shir (1973) and by Gibson and Launder (1978):

$$\Pi_{ij,w} = C_1' \frac{\varepsilon}{k}\left(R_{nn}\delta_{ij} - 3/2R_{ni}\delta_{nj} - 3/2R_{nj}\delta_{ni} \right) f + C_2' \frac{\varepsilon}{k}\left(\Pi_{nn,2}\delta_{ij} - 3/2\Pi_{ni,2}\delta_{nj} - 3/2\Pi_{nj,2}\delta_{ni} \right) f \tag{19}$$

where C_1' (= 0.5) and C_2' (= 0.1) are model coefficients and f (= $k^{1.5}/(x_n\varepsilon)$) is the wall damping function (here, x_n is the normal distance from the wall). Cokljat and Younis (1995) found good performance of eq.(19) in the simulation of various 2D boundary-layer flows. The damping effect of the free-surface is very similar to the solid boundary. In order to include the free-surface effects, we replace f with a term representing the free-surface damping function (f_{fs}) in eq.(19). Naot and Rodi (1982) proposed the free-surface damping function such as

$$f_{fs} = \left(\frac{L}{z_{fs}^{-1} + C_f L} \right)^2 \tag{20}$$

where C_f is a model parameter (= 0.16), z_{fs} is the normal distance from the free-surface, and L is the turbulence length scale defined by

$$L = \frac{C_\mu^{3/4} k^{3/2}}{\kappa\varepsilon} \tag{21}$$

where κ is von-Karman constant. In the present study, the free-surface is assumed to be flat, which is easy to estimate the normal distance from the free-surface.

The wall functions are used at the bottom boundary. For the Reynolds stresses, the zero gradient condition is applied, while the velocity gradients in the Reynolds stress terms are calculated by the logarithmic law. At the free-surface, the symmetry condition is imposed for all variables. However, for ε, the relationship by Rodi (1984) is prescribed in order to increase turbulence kinetic energy dissipation level at the free-surface. As for the lateral boundaries, we used the cyclic boundary condition. That is, the outlet flow conditions are used as the inlet conditions.

Using the computed flow structure, the coefficients of the form drag and skin friction are estimated, respectively, by

$$C_{ff} = \frac{p - p_{ref}}{(1/2)\rho U^2} \tag{22}$$

$$C_{fs} = \frac{\tau_w}{(1/2)\rho U^2} \tag{23}$$

where U is the mean velocity, τ_w is the wall

shear stress and p_{ref} is the reference pressure at the downstream boundary. The total resistance coefficient is the sum of the form drag and the skin friction which are averaged over the bedform length. That is,

$$C_F = C_{FF} + C_{FS} \tag{24}$$

where $C_{FF} = 1/L \cdot \int_0^L C_{ff} dx$ and $C_{FS} = 1/L \cdot \int_0^L C_{ff} dx$. The wall roughness is known to reduce the length of the separation eddy, which is due to the reduction of the negative wall shear stress. Thus, in rough open-channel flows, the wall roughness at the bottom boundary increases the magnitude of the skin friction.

3. CHARACTERISTICS OF BEDFORM GEOMETRY

Karim (1995) developed the following condition under which ripples or dunes are created by the flow:

$$Fr \le Fr_t \tag{25}$$

where Fr is the Froude number ($=U/\sqrt{gd}$) and Fr_t denotes the Froude number at the beginning of transition regime which is defined by

$$Fr_t = 2.716\left(\frac{d}{D_{50}}\right)^{-0.25} \tag{26}$$

where d is the mean water depth and D_{50} is the median diameter of sediment particles. According to Guy et al. (1966), ripples are formed on the bed when $N_* < 80$. Here, the dimensionless number N_* is defined by

$$N_* = \frac{u_* D_{50}}{\nu} \cdot \frac{U}{\sqrt{gRD_{50}}} \tag{27}$$

where u_* is the shear velocity, g is the gravitational acceleration, and R is the submerged specific gravity of sediment. When $N_* > 80$, dunes are formed on the channel bed. Karim (1999) proposed the following relationship for the bedform geometry:

$$\frac{h}{d} = \left\{\frac{\left[S - 0.0168(D_{50}/d)^{0.33} \cdot Fr^2\right](L/d)^{1.2}}{0.47Fr^2}\right\}^{0.73} \tag{28}$$

where h and L are the height and length of bedforms, respectively, and S is the energy slope. The respective lengths of ripple and dune are given by

$$L = 1{,}000 D_{50} \quad \text{for ripple bed} \tag{29}$$

$$L/d = 6.25 \quad \text{for dune bed} \tag{30}$$

which are proposed by Julien and Kaassen (1995) and by Yalin (1964), respectively.

4. APPLICATIONS

The RSM is applied to the experimental conditions in Lyn (1993), and the computed results are compared with the measurement data. Comparisons are also made with the numerical results by the $k-\omega$ model and by the $k-\varepsilon$ model. In the numerical simulation, mean water depth of H_o = 0.061 m and slope of S = 0.00145 are used with the bottom boundary condition of a rough surface with $k_s = D_{50}$ = 0.25 mm. The height (h) and length (L) of bedform are h = 0.012 m and L = 0.15 m, respectively.

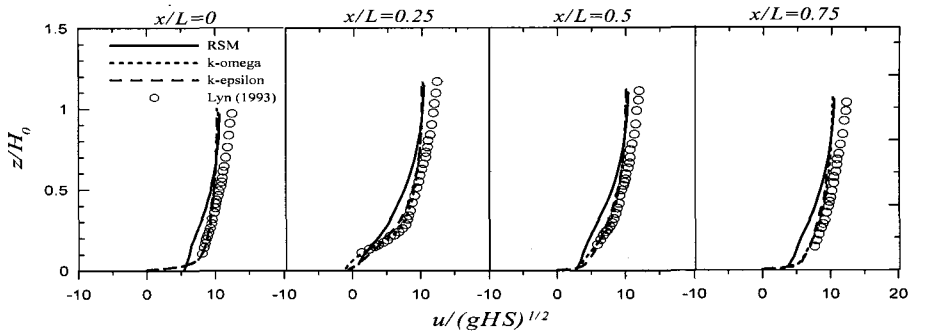

(a) *x*-Component Mean Velocity

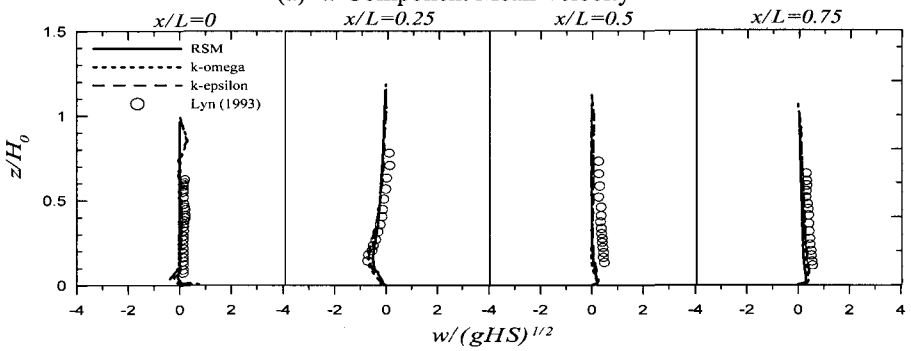

(b) *z*-Component Mean Velocity

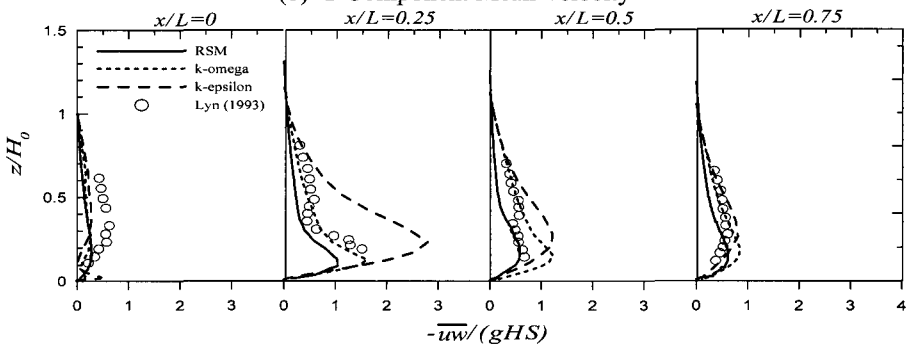

(c) Reynolds Stress

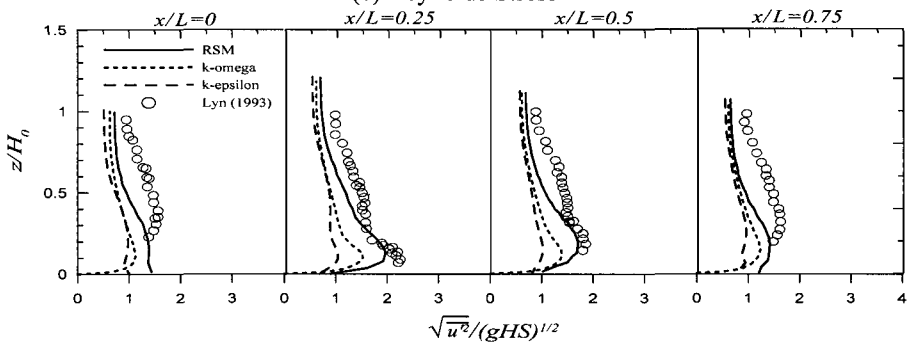

(d) Turbulence Intensity

Figure 2. Mean Flow and Turbulence Structures

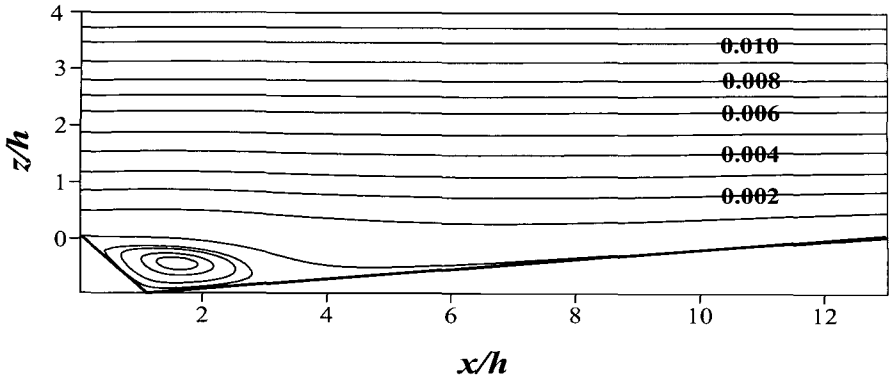

(a) RSM (Reattachment @ $x / h = 4.10$)

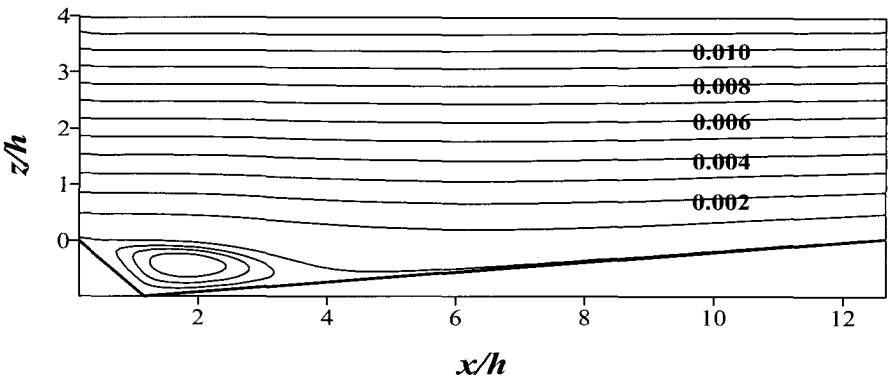

(b) $k-\omega$ model (Reattachment @ $x / h = 4.13$)

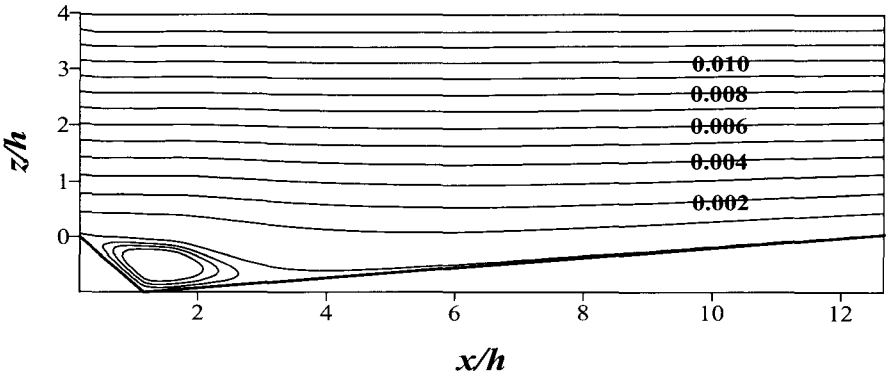

(c) $k-\varepsilon$ model (Reattachment @ $x / h = 3.75$)

Figure 3. Flow Separation and Reattachment over Bedform

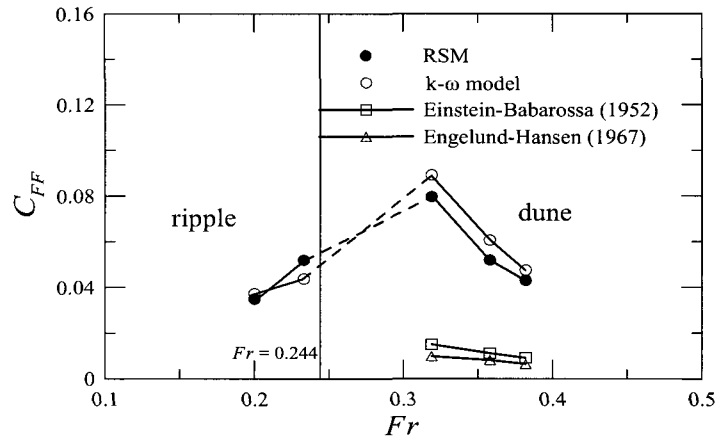

(a) Form Drag Coefficient

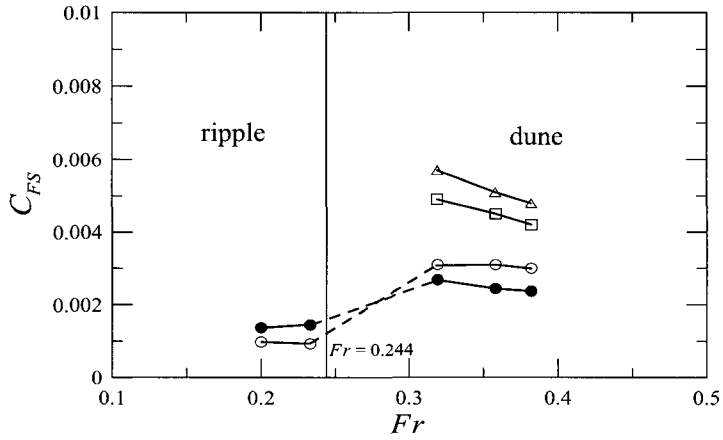

(b) Skin Friction Coefficient

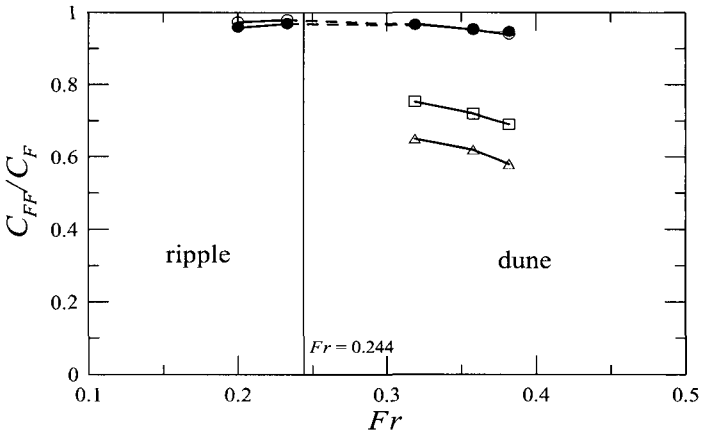

(c) Ratio of Form Drag Coefficient to Total Resistance Coefficient

Figure 4. Variation of Resistance Coefficients with Froude Number

Figures 2(a) and (b) show the distributions of x- and z-component mean velocities measured at four locations in the streamwise direction. In the figures, lines represent computed results by three turbulence models, and symbols denote profiles measured with laser Doppler velocimeter by Lyn (1993). The horizontal and the vertical axes are made dimensionless by shear velocity and mean flow depth, respectively. It is seen in Figure 2(a) that overall agreement between the predicted and the measured profiles is good. To be more precise, the simulated velocity profile by the RSM appears to be slightly smaller than other predictions and measured data. In Figure 2(b), the computed profiles of the mean velocity in the z-direction are nearly indistinguishable, and they agree well with the measured data.

The profiles of Reynolds stress are given in Figure 2(c). It is seen that the pattern of the measured profiles do not vary noticeably except the profile at $x/L = 0.25$. Note that the simulated results by the RSM and by the k-ω model are similar and match the measured data well. Whereas the k-ε model is observed to over- predict the Reynolds stress significantly at $x/L = 0.25$.

Figure 2(d) shows the turbulence intensity profiles. It is seen that all computed profiles are smaller than the measured data at all locations. However, it is observed that the results by the RSM match the observed data best. The turbulence intensity profiles predicted by the two-equation turbulence models appear to be similar and to be slightly smaller than the result by the RSM.

Figures 3(a)-(c) show the streamlines computed by the RSM, the $k-\omega$ model and the $k-\varepsilon$ model, respectively. In all figures, recirculation is clearly observed, i.e., the flow is separated at the crest of bedform and it is reattached after some distance. The computed separation lengths of eddy are x/h = 4.10, 4.13, and 3.75 in the results of the RSM, the $k-\omega$ model, and the $k-\varepsilon$ model, respectively. In general, the skin friction decreases as the separation length increases.

Figure 4 shows the variation in resistance coefficients with respect to Froude number when the median size of sediment particles and the energy slope are kept constant. In order to determine the water depth, which is a function of resistance, we use Einstein-Babarossa formula in the dune regime. In the ripple regime, since the empirical relationship is not available, we use iterations by using the numerical model (the computations converge within 5 iterations in most cases). The ranges of flow variables are 0.1-0.2 m^2/s for the discharge, 0.25- 0.32 m for the water depth, and 0.37-0.67 m/s for the mean velocity.

It is seen in Figure 4(a) that, as Froude number increases, the computed value of the form drag increases in the ripple regime, and it increases abruptly in the transition region. Then the coefficient decreases in the dune regime. Compared with the empirical formulas in the dune regime, the predicted values of the form drag are much larger than those from the empirical formulas. In Figure 4(b), the computed values of the skin friction in both ripple and dune regimes are seen to be constant with Froude number. In contrast, it is found that the numerical simulations provide the skin friction coefficients smaller than the values from the empirical formulas. Figure 4(c) shows the contribution of the form drag to the total resistance. According to the empirical formulas, it appears that 60-80% of the total resistance comes from the form drag. Whereas the numerical model

predicts that over 90% of the total resistance is due to the form drag.

Comparing two simulated results, the form drag computed by the RSM is slightly smaller than that by the k-ω model in the dune regime. The calculated skin friction by the RSM seems to be a little larger than the values by the k-ω model in the ripple regime. On the contrary, it is seen that the k-ω model yields larger skin frictions in the dune regime. This leads to a similar level of contribution of the form drag to the total resistance in both predictions.

5. CONCLUSIONS

Recent development of computational fluid dynamics enables us to simulate the detailed mechanism of the flow over bedform. However, it is known that the numerical model based upon the two-equation turbulence closures such as the k-ε model and the k-ω model over- and under-predict the form drag and the skin friction, respectively, compared with the empirical relationships (Yoon and Patel, 1996). Non-isotropic effect of turbulence, ignorance of particle movement over bedform, and movement of bedform in the downstream direction, and 3D bedform geometry may be responsible for this problem.

This paper presented a non-isotropic turbulence modeling of flows over bedforms. The Reynolds stress model was used for the turbulence closure. In the modeling, we used Launder, Reece, and Rodi's model for the pressure strain correlation term and the Hanjalic and Launder's model for the diffusion term. We applied the developed model to the experimental measurement, and found the model improves the mean flow and turbulence structure slightly compared with the two-equation turbulence models. It was also observed that the separation length of eddy computed by the Reynolds stress model lies between the results by the k-ε model and the k-ω model. By using the model, the form drag and the skin friction were estimated for flows at different Froude numbers. It was found that the form drag and the skin friction are still over- and under-estimated by the Reynolds stress model, respectively, compared with the empirical formulas.

ACKNOWLEDGMENT

This work was supported by Korea Research Foundation Grant (KRF-2000-003-E00538).

REFERENCES

Choi, S.-U., Kim, J., and Kang, H. (2002). "Numerical assessment of impact of bedform geometry on flow resistance." *4th International Ecohydraulics Symposium*, Cape Town, South Africa.

Cokljat, D. and Younis, B.A. (1995). "Second-order closure study of open-channel flows." *Journal of Hydraulic Engineering*, ASCE, 121(2), 94-107.

Einstein, H.A. and Barbarossa, N.L. (1952). "River channel roughness." *Transactions of the American Society of Civil Engineering*, ASCE, 117, 1121-1146.

Engelund, F. and Hansen, E. (1967). *A Monograph on Sediment Transport in Alluvial Streams*, Teknisk Vorlag, Copenhagen, Denmark.

Gibson, M.M. and Launder, B.E. (1978). "Ground effects on pressure fluctuations in the atmospheric boundary layer." *Journal of Fluid Mechanics*, 86, 491-511.

Guy, H.P., Simons, D.B., and Richardson, E.V. (1966). "Summary of alluvial channel data from flume experiments, 1956-1961."

Geological Survey Profl. Paper 462-I, U.S. Department of the Interior, Washington, D.C.

Hanjalic, K. and Launder, B.E. (1972). "A Reynolds stress model of turbulence and its application to thin shear flows." *Journal of Fluid Mechanics*, 52(4), 609-638.

Julien, P.Y. and Klaassen, G.J. (1995). "Sand-dune geometry of large rivers during floods." *Journal of Hydraulic Engineering*, ASCE, 121(9), 657-663.

Karim, F. (1995). "Bed configuration and hydraulic resistance in alluvial channel flows." *Journal of Hydraulic Engineering*, ASCE, 121(1), 15-25.

Karim, F. (1999). "Bed-form geometry in sand-bed flows." *Journal of Hydraulic Engineering*, ASCE, 125(12), 1253-1261.

Launder, B.E., Reece, G.J., and Rodi, W. (1975). "Progress in the development of Reynolds stress turbulence closure." *Journal of Fluid Mechanics*, 63(3), 537-566.

Launder, B.E. and Spaling, D.B. (1974). "The numerical computation of turbulent flow." *Computational Methods in Applied Mechanics*, 3, 269-289.

Lyn, D.A. (1993). "Turbulence measurement in open-channel flows over artificial bedforms." *Journal of Hydraulic Engineering*, ASCE, 119(3), 306-326.

Naot, D. and Rodi, W. (1982). "Calculation of secondary currents in channel flow." *Journal of the Hydraulics Division*, ASCE, 108(8), 948-968.

Rodi, W. (1984). *Turbulence Modeling and Their application in Hydraulics. Monograph*, IAHR, Delft, The Netherlands.

Rotta, J.C. (1951). "Statistical theorie nichthomogener turbulenz." *Zeitschift f. Physik*, 131, 51-77.

Shir, C.C. (1973). "A preliminary numerical study of atmospheric turbulent flow in the idealized planetary boundary layer." *Journal of Atmospheric Sciences*, 30, 1327-1339.

Wilcox, D.C. (1988). "Reassessment of the scale determining equation for advanced turbulence models." *AIAA Journal*, 26(11), 1299-1310.

Yalin, M.S. (1964). "Geometrical properties of sand waves." *Journal of the Hydraulics Division*, ASCE, 90(5).

Yoon, J.Y. and Patel, V.C. (1996). "Numerical model of turbulent flow over sand dune." *Journal of Hydraulic Engineering*, ASCE, 122(1), 10-18.

Associate Professor, School of Civil & Environmental Engineering, Yonsei University, Seoul 120-749, Korea

(E-mail : schoi@yonsei.ac.kr)

Graduate Student, School of Civil & Environmental Engineering, Yonsei University, Seoul 120-749, Korea

(E-mail : kanghs@yonsei.ac.kr)